

## LIGHT INDUCED MICROWAVE OSCILLATOR

X. Steve Yao and Lute Maleki  
Jet Propulsion Laboratory, California Institute of Technology  
4800 Oak Grove Dr., Pasadena, CA 91109  
(818) 393-9031, Fax: (818) 393-6773  
E-mail: xsyao@fridge.jpl.nasa.gov

## ABSTRACT

We describe a novel oscillator that converts continuous light energy into stable and spectrally pure microwave signals. This Light Induced Microwave Oscillator, LIMO, consists of a pump laser and a feedback circuit including an intensity modulator, an optical fiber delay line, a photodetector, an amplifier, and a filter. We develop a quasi-linear theory and obtain expressions for the threshold condition, the amplitude, the frequency, the linewidth, and the spectral power density of the oscillation. We also present experimental data to compare with the theoretical results. Our findings indicate that the LIMO can generate ultra-stable, spectrally pure microwave reference signals up to 75 GHz with a phase noise lower than -140 dBc/Hz at 10 KHz.

## INTRODUCTION

Oscillators are devices that convert energy from a continuous source to a periodically varying signal. They represent the physical realization of a fundamental basis of all physics, the harmonic oscillator, and they are perhaps the most widely used devices in the modern day society. Today a variety of mechanical<sup>1</sup> (such as the pendulum), electromagnetic (such as LC<sup>2,3</sup> and cavity based<sup>4</sup>), and atomic (such as masers<sup>5</sup> and lasers<sup>6</sup>) oscillators provide a diverse range in the approximation to the realization of the ideal harmonic oscillator. The degree of the spectral purity and stability of the output signal of the oscillator is the measure of the accuracy of this approximation, and is fundamentally dependent on the energy storage ability of the oscillator, determined by the resistive loss (generally frequency dependent) of the various elements in the oscillator.

An important type of oscillator widely used today is the electronic oscillator. The first such oscillator was invented by L. DeForest<sup>2</sup> in 1912, shortly after the development of the vacuum tube. In this triode based device known as the "van der Pol oscillators" the flux of electrons emitted by the cathode and flowing to the anode is modulated by the potential on the intervening grid. This potential is derived from the feedback of the current in the anode circuit containing an energy storage element (i.e., the frequency selecting LC filter) to the grid, as shown in Fig. 1a.

Today the solid state counterparts of these "valve" oscillators based on transistors are pervasive in virtually every application of electronic devices, instruments, and systems. Despite their widespread use, electronic oscillators, whether of the vacuum tube or the solid state variety, are relatively noisy and lack adequate stability for applications where very high stability and spectral purity are required. The limitation to the performance of electronic oscillators is due to ohmic and dispersive losses in various elements in the oscillator including the LC resonant circuit.

For approximately the past fifty years the practice of reducing the noise in the electronic oscillator by combining it with a high quality factor (Q) resonator has been followed to achieve improved stability and spectral purity. The Q is a figure of merit for the resonator given by  $Q = 2\pi f\tau_d$  where  $\tau_d$  is the energy decay time that measures the energy storage ability of the resonator and  $f$  is the resonant frequency. High Q

resonators used for stabilization of the electronic oscillator include mechanical resonators, such as quartz crystals<sup>7,8</sup>, electromagnetic resonators, such as dielectric cavities,<sup>9</sup> and acoustic<sup>10</sup> and electrical delay lines, where the delay time is equivalent to the energy decay time  $\tau_d$  and determines the achievable  $Q$ . This combination with a resonator results in hybrid type oscillators referred to as electromechanical, electromagnetic, or electro-acoustic, depending on the particular resonator used with the oscillator circuit. The choice of the particular resonator is generally determined by a variety of factors, but for the highest achievable  $Q$ 's at room temperatures the crystal quartz is the resonator of choice for the stabilization of the electronic oscillator. However, because quartz resonators have only a few high  $Q$  resonant modes at low frequencies,<sup>7,8</sup> they have limited range of frequency tunability and cannot be used to directly generate high frequency signals.

in this paper we introduce a novel photonic oscillator<sup>1,12</sup> characterized by spectral purity and frequency stability rivaling the best crystal oscillators. This oscillator, shown schematically in Fig. 1b, is based on converting the continuous light energy from a pump laser to radio frequency (RF) and microwave signals, and thus we refer to it with the acronym LIMO for the Light Induced Microwave Oscillator. The LIMO is fundamentally similar to the van der Pol oscillator with photons replacing the function of electrons, an electro-optic (E/O) modulator replacing the function of the grid, and a photodetector replacing the function of the anode. The energy storage function of the LC circuit in the van der Pol oscillator is replaced with a long fiber optic delay line in the LIMO.

Despite this close similarity, the LIMO is characterized by significantly lower noise and very high stability, as well as other functional characteristics which are not achieved with the electronic oscillator. The superior performance of the LIMO results from the use of electro-optic and photonic components which are generally characterized with high efficiency, high speed, and low dispersion in the microwave frequency regime. Specifically, currently there are photodetectors available with as high as 90% quantum efficiency, and can respond to signals with frequencies as high as 110 GHz.<sup>13</sup> Similarly, E/O modulators with 75 GHz frequency response are also available.<sup>14</sup> Finally, the commercially available optical fiber which has a small loss of 0.2 dB/km for 1550 nm light allows long storage time of the optical energy with negligible dispersive loss (loss dependent on frequency) for the intensity modulations at microwave frequencies.

The LIMO may also be considered as a hybrid oscillator in so far as its operation involves both light energy and microwave signals. Nevertheless as a hybrid oscillator, the LIMO is unique in that its output may be obtained both directly as a microwave signal, or as intensity modulation of a optical carrier. This property of the LIMO is quite important for applications involving optical elements, devices, or systems.<sup>12</sup>

The ring configuration consisting of an electro-optic modulator which is fed back with a signal from the detected light at its output has been previously studied by a number of investigators interested in the nonlinear dynamics of bistable optical devices.<sup>5-19</sup> The use of this configuration as a possible oscillator was first suggested by A. Neyer and E. Voges.<sup>20</sup> The interest of their investigations was however primarily focused on the nonlinear regime and the chaotic dynamics of the oscillator. This same interest persisted in the work of T. Aida and D. Davis,<sup>21</sup> who used a fiber wave guide as a delay line in the loop. Our studies, by contrast, are specifically focused on the stable oscillation dynamics and the noise properties of the oscillator. The sustainable quasi-linear dynamics, both in our theoretical and experimental demonstrations, are arrived at by the inclusion of a filter in the feedback loop to eliminate harmonics generated by the nonlinear response of the E/O modulator. This approach yields stable, low noise oscillations which closely supports the analytical formulation presented here.

In this paper we first describe the oscillator and identify the physical basis for its operation. We then develop a quasi-linear theory for the oscillator dynamics, and for the oscillator noise. Results of the theory is then compared with experimental results.

## DESCRIPTION OF THE OSCILLATOR

The LIMO utilizes the transmission characteristics of a modulator together with a fiber optic delay line to convert light energy into stable, spectrally pure RF/microwave reference signals. A detailed construction of the oscillator is shown schematically in Fig. 2. In this depiction, light from a laser is introduced into an E/O modulator, the output of which is passed through a long optical fiber, and detected with a photodetector. The output of the photodetector is amplified and filtered and fed back to the electric port of the modulator. This configuration supports self sustained oscillations, at a frequency determined by the fiber delay length, bias

setting of the modulator, and the bandpass characteristics of the filter. It also provides for both electric and optical outputs, a feature which is of considerable advantage to photonics applications.

We use a regenerative feedback approach to analyze the spectral properties of the LIMO. Similar methods have been successfully used to analyze lasers<sup>5</sup> and surface acoustic wave oscillators.<sup>22</sup> The conditions for self sustained oscillations include coherent addition of partial waves each way around the loop, and a loop gain exceeding losses for the circulating waves in the loop. The first condition implies that all signals that differ in phase by some multiple of  $2\pi$  from the fundamental signal may be sustained. Thus the oscillation frequency is limited only by the characteristic frequency response of the modulator, and the setting of the filter, which eliminates all other sustainable oscillations. The second condition implies that with adequate light input power, self sustained oscillations may be obtained, without the need for the RF/microwave amplifier in the loop. These characteristics, expected based on the qualitative analysis of the oscillator dynamics, are mathematically derived in the following sections.

## QUASI-LINEAR THEORY OF THE LIMO

In the following sections we introduce a quasi-linear theory to study the dynamics and noise of a LIMO. In the discussion, we assume that the E/O modulator in the oscillator is of the Mach-Zehnder type. However, the analysis of oscillators made with different E/O modulators may follow the same procedure. The flow of the theory is as follows. First the open loop characteristics of a photonic link consisting of a laser, a modulator, a fiber delay, and photodetector is determined. We then close the loop back into the modulator and invoke a quasi-linear analysis by including a filter in the loop. This approach leads us to a formulation for the amplitude and the frequency of the oscillation. In the next step we consider the influence of the noise in the oscillator, again assisted by the presence of the filter which limits the number of circulating Fourier components. We finally arrive at an expression for the spectral density of the LIMO which would be suitable for experimental investigations.

### A. Oscillation Threshold

The optical power from the E/O modulator's output port that forms the loop is related to an applied voltage  $V_{in}(t)$  by:

$$P(t) = (\alpha P_o / 2) \{1 - \eta \sin \pi [V_{in}(t) / V_\pi + V_B / V_\pi]\}, \quad (1)$$

where  $\alpha$  is the fractional insertion loss of the modulator,  $V_\pi$  is its half wave voltage,  $V_B$  is its bias voltage,  $P_o$  is the input optical power, and  $\eta$  determines the extinction ratio of the modulator by  $(1 + \eta) / (1 - \eta)$ .

If the optical signal  $P(t)$  is converted to an electric signal by a photodetector, the output electric signal after an RF amplifier is:

$$V_{out}(t) = \rho P(t) R G_A = V_{ph} \{1 - \eta \sin \pi [V_{in}(t) / V_\pi + V_B / V_\pi]\} \quad (2)$$

where  $\rho$  is the responsivity of the detector,  $R$  is the load impedance of the photodetector,  $G_A$  is the amplifier's voltage gain, and  $V_{ph}$  is the photovoltage defined as:

$$V_{ph} = (\alpha P_o \rho / 2) R G_A = I_{ph} R G_A, \quad (3)$$

with  $I_{ph} \equiv \alpha P_o \rho / 2$  as the photocurrent. The LIMO is formed by feeding the signal of Eq. (2) back to the RF input port of the E/O modulator. Therefore the small signal open loop gain  $G_S$  of the LIMO is:

$$G_S \equiv \left. \frac{dV_{out}}{dV_{in}} \right|_{V_{in}=0} = - \frac{\eta \pi V_{ph}}{V_\pi} \cos\left(\frac{\pi V_B}{V_\pi}\right) \quad (4)$$

The highest small signal gain is obtained when the modulator is biased at quadrature, that is when  $V_B = 0$  or  $V_\pi$ . From Eq. (4) one may see that  $G_S$  can be either positive or negative, depending on the bias voltage. The modulator is said to be positively biased if  $G_S > 0$ , otherwise is negatively biased. Therefore, when  $V_B = 0$ , the modulator is biased at negative quadrature, while when  $V_B = V_\pi$ , the modulator is biased at positive quadrature. Note that in most externally modulated photonic links, the E/O modulators can be biased at either positive or negative quadrature without affecting its performance. However, as will be seen next, the biasing polarity will have an important effect on the operation of the LIMO.

In order for the LIMO to oscillate, the magnitude of the small signal open loop gain must be larger than unity. From Eq. (4) we immediately obtain the oscillation threshold of the LIMO to be:

$$V_{ph} = V_{\pi} / [\pi \eta |\cos(\pi V_B / V_{\pi})|] \quad (5)$$

For the ideal case in which  $\eta = 1$  and  $V_B = 0$  or  $V_{\pi}$ , Eq. (5) becomes:

$$V_{ph} = V_{\pi} / \pi \quad (6)$$

It is important to notice from Eq. (3) and Eq. (6) that the amplifier in the loop is not a necessary condition for oscillation. So long as  $I_{ph} R \geq V_{\pi} / \pi$  is satisfied, no amplifier is needed ( $G_A = 1$ ). It is the optical power from the pump laser that actually supplies the necessary energy for the LIMO. This property is of practical significance because it enables the LIMO to be powered remotely using an optical fiber. Perhaps more significantly, however, the elimination of the amplifier in the loop also eliminates the amplifier noise, resulting in a more stable oscillator. For a modulator with a  $V_{\pi}$  of 3.14 volts and an impedance  $R$  of  $50 \Omega$ , a photocurrent of 20 mA is required for sustaining the photonic oscillation without an amplifier. This corresponds to an optical power of 25 mW, assuming the responsivity  $p$  of the photodetector to be 0.8 A/W.

### B. Linearization Of the E/O Modulators Response Function

in general, Eq. (2) is nonlinear. If the electrical input signal  $V_{in}(t)$  to the modulator is a sinusoidal wave with an angular frequency of  $\omega$ , an amplitude of  $V_o$ , and an initial phase  $\beta$ :

$$V_{in}(t) = V_o \sin(\omega t + \beta), \quad (7)$$

the output at the photodetector,  $V_{out}(t)$ , can be obtained by substituting Eq. (7) in Eq. (2) and expanding the left hand side of Eq. (2) with Bessel functions

$$\begin{aligned} V_{out}(t) = V_{ph} \{ & 1 - \eta \sin\left(\frac{\pi V_B}{V_{\pi}}\right) \left[ J_0\left(\frac{\pi V_o}{V_{\pi}}\right) + 2 \sum_{m=1}^{\infty} J_{2m}\left(\frac{\pi V_o}{V_{\pi}}\right) \cos(2m\omega t + 2m\beta) \right] \right. \\ & \left. - 2\eta \cos\left(\frac{\pi V_B}{V_{\pi}}\right) \sum_{m=0}^{\infty} J_{2m+1}\left(\frac{\pi V_o}{V_{\pi}}\right) \sin[(2m+1)\omega t + (2m+1)\beta] \right\} \end{aligned} \quad (8)$$

It is clear from Eq. (8) that the output contains many harmonic components of  $\omega$ .

The output can be linearized if it passes through an RF filter with a bandwidth sufficiently narrow to block all harmonic components. The linearized output can be easily obtained from Eq. (8) to be:

$$V_{out}(t) = G(V_o)V_{in}(t) \quad (9a)$$

where the voltage gain coefficient  $G(V_o)$  is defined as:

$$G(V_o) = G_s \frac{2V_\pi}{\pi V_o} J_1\left(\frac{\pi V_o}{V_\pi}\right). \quad (10a)$$

It can be seen that the voltage gain ' $G(V_o)$ ' is a nonlinear function of the input amplitude  $V_o$  and its magnitude decreases monotonically with  $V_o$ . However, for a small enough input signal ( $V_o \ll V_\pi$  and  $J_1(\pi V_o/V_\pi) \approx \pi V_o/2V_\pi$ ), we can recover from Eq. (10a) the small signal gain:  $G(V_o) \approx G_s$ .

If we expand the left hand side of Eq. (2) with Taylor series, the gain coefficient can be obtained as:

$$G(V_o) = G_s \left[ 1 - \frac{1}{2} \left( \frac{\pi V_o}{2V_\pi} \right)^2 + \frac{1}{12} \left( \frac{\pi V_o}{2V_\pi} \right)^4 \right] \quad (10b)$$

It should be kept in mind that in general,  $G(V_o)$  is also a function of the frequency  $\omega$  of the input signal, because  $V_{ph}$  is linearly proportional to the gain of the RF amplifier and the responsivity of the photodetector, which are all frequency dependent. In addition, the  $V_\pi$  of the modulator is also a function of the input RF frequency. Furthermore, the frequency response of the RF filter in the loop can also be lumped into  $G(V_o)$ . In the discussions below, we will introduce a unitless complex filter function  $\tilde{F}(\omega)$  to explicitly account for the combined effect of all frequency dependent components in the loop while treating  $G(V_o)$  to be frequency independent:

$$\tilde{F}(\omega) = F(\omega)e^{i\phi(\omega)}, \quad (11)$$

where  $\phi(\omega)$  is the frequency dependent phase caused by the dispersive component in the loop and  $F(\omega)$  is the real normalized transmission function. Now Eq. (9a) can be rewritten in complex form as:

$$\tilde{V}_{out}(t) = \tilde{F}(\omega)G(V_o)\tilde{V}_{in}(\omega, t), \quad (9b)$$



where  $\tilde{V}_{out}(t)$  are complex input and output voltages. Note that although Eq. (9b) is linear, the nonlinear effect of the modulator is not lost -- it is contained in the nonlinear gain coefficient  $G(V_o)$ .

### C. Oscillation Frequency And Amplitude

In this section we derive the expressions for the amplitude and frequency of LIMO. Like other oscillators, the oscillation of a LIMO starts from noise transient, which is then built up and sustained with feedback at the level of the oscillator output signal. We derive the amplitude of the oscillating signal by considering this process mathematically. The noise transient can be viewed as a collection of sine waves with random phases and amplitudes. To simplify our derivation, we use this noise input with the linearized expression Eq. (9b) for the loop response. Because Eq. (9b) is linear, the superposition principle holds and we can analyze the response of the LIMO by first inspecting the influence of a single frequency component of the noise spectrum:

$$\tilde{V}_n(\omega, t) = \tilde{V}_n(\omega) e^{i\omega t}, \quad (12)$$

where  $\tilde{V}_n(\omega)$  is a complex amplitude of the frequency component.

Once the noise component of Eq. (12) is in the oscillator, it would circulate in the loop and the recurrence relation of the fields from Eq. (9b) is:

$$\tilde{V}_n(\omega, t) = \tilde{F}(\omega) G(V_o) \tilde{V}_{n-1}(\omega, t - \tau'), \quad (13)$$

where  $\tau'$  is the time delay resulting from the physical length of the feedback and  $n$  is the number of times the field has circulated around the loop, with  $\tilde{V}_{n=0}(\omega, t) = \tilde{V}_n(\omega, t)$ . In Eq. (13), the argument  $V_o$  in  $G(V_o)$  is the amplitude of the total field (the sum of all circulating fields) in the loop.

The total field at any instant of time is the summation of all circulating fields. Therefore, with the input of Eq. (12) injected in the oscillator, the signal measured at the RF input to the modulator for the case that the open loop gain is less than unity can be expressed as:

$$\tilde{V}(\omega, t) = G_a \tilde{V}_n(\omega) \sum_{n=0}^{\infty} [\tilde{F}(\omega) G(V_o) e^{i\omega(t-n\tau')}] = \frac{G_a \tilde{V}_n e^{i\omega t}}{1 - \tilde{F}(\omega) G(V_o) e^{-i\omega\tau'}} \quad (14)$$

For loop gain below threshold and with  $V_o$  small,  $G(V_o)$  is essentially the small signal gain  $G_s$  given by Eq. (4)

The corresponding RF power of the circulating noise at frequency  $\omega$  is therefore:

$$P(\omega) = \frac{I \tilde{V}(\omega, t)^2}{2R} = \frac{G_s^2 |\tilde{V}_{in}(\omega)|^2 / (2R)}{1 + |F(\omega) G(V_o)| - 2F(\omega) |G(V_o)| \cos[\omega\tau + \phi(\omega) + \phi_o]}, \quad (15)$$

where  $\phi_o = 0$  if  $G(V_o) > 0$  and  $\phi_o = \pi$  if  $G(V_o) < 0$ .

For a constant  $\tilde{V}_{in}(\omega)$ , the frequency response of a LIMO has equally spaced peaks similar to that of a Fabry-Perot resonator, as shown in Fig. 3. These peaks are located at the frequencies determined by:

$$\omega_k \tau + \phi(\omega_k) + \phi_o = 2k\pi \quad k = 0, 1, 2, \dots, \quad (16)$$

where  $k$  is the mode number. In Fig. 3, each peak corresponds to a frequency component resulting from the coherent summation of all circulating fields in the loop at that frequency. As the open loop gain increases, the magnitude of each peak becomes larger and its shape becomes sharper. These peaks are the possible oscillation modes of the LIMO. When the open loop gain is larger than unity, each time a noise component at a peak frequency travels around the loop, it is amplified and its amplitude increases geometrically -- an oscillation is started from noise.

Because an RF filter is placed in the loop, the gain of only one mode is allowed to be larger than unity, thus selecting the mode that is allowed to oscillate. Because of the nonlinearity of the E/O modulator or the RF amplifier, the amplitude of the oscillation mode cannot increase indefinitely. As the amplitude increases, higher harmonics of the oscillation will be generated by the nonlinear effect of the modulator or the amplifier, at the expense of the oscillation power, and these higher harmonics will be filtered out by the RF filter. Effectively, the gain of the oscillation mode is decreased according to Eq. (10) till the gain is, for all practical measures, equal to unity, and the oscillation is stable. As will be shown later, because of the continuous presence of noise, the closed loop gain of an oscillating mode is actually less than unity by a tiny amount on the order of  $10^{-10}$ , which ensures that the summation in Eq. (14) converges.

in the discussion follows only one mode  $k$  is allowed to oscillate, and so we will denote the oscillation frequency of this mode as  $f_{osc}$  or  $\omega_{osc}$  ( $\omega_{osc} = 2\pi f_{osc}$ ), its oscillation amplitude as  $V_{osc}$ , and its oscillation power as  $P_{osc}$  ( $P_{osc} = V_{osc}^2/2R$ ). In this case, the amplitude  $V$  of total field in Eq. (15) is just the oscillation amplitude  $V_{osc}$  of the oscillating mode. If we choose the transmission peak of the filter to be at the oscillation frequency  $\omega_{osc}$  and so  $H(\omega_{osc}) = 1$ , the oscillation amplitude can be solved by setting the gain coefficient  $|G(V_{osc})|$  in Eq. (15) be unity. From Eq. (10a) it leads to:

$$|J_1\left(\frac{\pi V_{osc}}{V_\pi}\right)| = \frac{1}{2|G_s|} \frac{\pi V_{osc}}{V_\pi}, \quad (17a)$$

In deriving Eq. (17a), we have assumed that the RF amplifier in the loop is linear enough that the oscillation power is limited by the nonlinearity of the E/O modulator. The amplitude of the oscillation can be obtained by solving Eq. (17a) graphically, and the result is shown in Fig. 4a. Note that this result is the same as that obtained by Neyer and Voges<sup>20</sup> using a more complicated approach.

If we use Eq. (10b), we can obtain the approximated solution of the oscillation amplitude to be:

$$V_{osc} = \frac{2\sqrt{2}V_\pi}{\pi} \sqrt{1 - \frac{1}{|G_s|}} \quad \text{3rd order expansion} \quad (17b)$$

$$V_{osc} = \frac{2\sqrt{3}V_\pi}{\pi} \left( 1 - \frac{1}{\sqrt{3}} \sqrt{\frac{4}{|G_s|} - 1} \right)^{1/2} \quad \text{5th order expansion} \quad (17c)$$

The threshold condition of  $|G_s| \geq 1$  is clearly indicated in Eq. (17b) and Eq. (17c). Fig. 4a shows the normalized oscillation amplitude as a function of  $|G_s|$  obtained from Eq. (17a), Eq. (17b) and Eq. (17c) respectively. Comparing the three theoretical curves one can see that for  $|G_s| \leq 1.5$ , the 3rd order expansion result is a good approximation. For  $|G_s| \leq 3$ , the fifth order expansion result is a good approximation.

The corresponding oscillation frequency  $f_{osc} = f_k = \omega_k/2\pi$  can be obtained from Eq. (16) to be:

$$f_{osc} = f_k = (k + 1/2)/\tau \quad \text{for } G(V_{osc}) < 0, \quad (18a)$$

$$f_{osc} = f_k = k/\tau \quad \text{for } G(V_{osc}) > 0, \quad (18b)$$

where  $\tau$  is the total group delay of the loop, including the physical length delay  $\tau'$  of the loop and the group delay resulting from dispersive components (such as an amplifier) in the loop, and it is given by:

$$\tau = \tau' + \left. \frac{d\phi(\omega)}{d\omega} \right|_{\omega = \omega_{osc}} \quad (19)$$

For all practical purposes,  $J_1(\pi V_{osc}/V_\pi) \geq 0$  or  $V_{osc}/V_\pi < 1.2, 1$  and the sign of  $G(V_{osc})$  is determined by the small signal gain  $G_s$ . It is interesting to notice from Eq. (18) that the oscillation frequency depends on the biasing polarity of modulator. For negative biasing ( $G_s < 0$ ), the fundamental frequency is  $1/(2\tau)$ , while for positive biasing ( $G_s > 0$ ), the fundamental frequency is doubled to  $1/\tau$ .

#### D. The Spectrum

The fundamental noise in a LIMO consists of the thermal noise, the shot noise, and the laser's intensity noise, which for the purpose of analysis can be viewed as all originating from the photodetector. Since the photodetector is directly connected to the amplifier, the noise can be viewed as entering the oscillator at the input of the amplifier, as shown in Fig. 2.

We compute the spectrum of the oscillator signal by determining the power spectral density of noise in the oscillator. Let  $\rho_N(\omega)$  be the power density of the input noise at frequency  $\omega$ , we have

$$\rho_N(\omega)\Delta f = \frac{|\tilde{V}_{in}(\omega)|^2}{2R}, \quad (20)$$

where  $\Delta f$  is the frequency bandwidth. Substituting Eq. (20) in Eq. (15) and letting  $F(\omega_{osc}) = 1$ , we obtain the power spectral density of the oscillating mode  $k$  to be:

$$S_{RF}(f') = \frac{P(f')}{\Delta f P_{osc}} = \frac{\rho_N G_A^2 / P_{osc}}{1 + |F(f')G(V_{osc})|^2 - 2F(f')|G(V_{osc})|\cos(2\pi f' \tau)}, \quad (21)$$

where  $f' \equiv (\omega - \omega_{osc})/2\pi$  is the frequency offset from the oscillation peak  $f_{osc}$ . In deriving Eq. (21), both Eq. (16) and Eq. (19) are used.

By using the normalization condition

$$\int_{-\infty}^{\infty} S_{RF}(f') df' \approx \int_{-1/2\tau}^{1/2\tau} S_{RF}(f') df' = 1, \quad (22)$$

we obtain

$$1 - |G(V_{osc})|^2 \approx 2[1 - |G(V_{osc})|] = \frac{\rho_N G_A^2}{\tau P_{osc}} \quad (23)$$

Note that in Eq. (22), we have assumed that the spectral width of the oscillating mode is much smaller than the mode spacing  $1/\tau$  of the oscillator, so that the integration over  $1/\tau$  is sufficiently accurate. In addition, in the derivation we have assumed that  $|F(f')| \approx 1$  in the frequency band of integration.

Typically,  $\rho_N = 10^{-17}$  mW/Hz,  $P_{osc} = 10$  mW,  $G_A^2 \sim 100$ , and  $\tau = 10^{-6}$  s. From Eq. (23) one can see that the closed loop gain  $|G(V_{osc})|$  of the oscillating mode is less than unity by an amount of  $10^{-10}$ . Therefore the equation  $|G(V_{osc})| \approx 1$  is sufficiently accurate for calculating the oscillation amplitude  $V_{osc}$ , as proceeded in Eq. (17).

Finally, substituting Eq. (23) in Eq. (21), we obtain the RF spectral density of the LIMO to be:

$$S_{RF}(f') = \frac{\delta}{(2 - \delta/\tau) - 2\sqrt{1 - 3/2\cos(2\pi f'\tau)}} \quad (24a)$$

where  $\delta$  is defined as:

$$\delta \equiv \rho_N G_A^2 / P_{osc} \quad (25)$$

As mentioned before,  $\rho_N$  is the equivalent input noise density injected into the oscillator from the input port of the amplifier and  $P_{osc}/G_A^2$  is the total oscillating power measured before the amplifier. Here  $\delta$  is the input noise-to-signal ratio to the oscillator.

For the case where  $2\pi f'\tau \ll 1$ , we can simplify Eq. (24a) by expanding the cosine function in Taylor series:

$$S_{RF}(f') = \frac{\delta}{(\delta/2\tau)^2 + (2\pi)^2 (\tau f')^2} \quad (24b)$$

Eq. (24b) is a good approximation even for  $2\pi f'\tau = 0.7$  at which value the error resulted from neglecting the higher order terms in Taylor expansion is less than 1 o/o.

It can be seen from Eq. (24b) that the spectral density of the oscillating mode is a Lorentzian function of frequency. Its full width at half maximum (FWHM)  $\Delta f_{FWHM}$  is

$$\Delta f_{FWHM} = \frac{1}{2\pi} \frac{\delta}{\tau^2} = \frac{1}{2\pi} \frac{G_A^2 \rho_N}{\tau^2 P_{osc}}, \quad (26a)$$

It is evident from Eq. (26a) that  $\Delta f_{FWHM}$  is inversely proportional to the square of loop delay time and linearly proportional to the input noise to signal ratio  $\delta$ . For a typical  $\delta$  of  $10^{-16}/\text{Hz}$  and a loop delay of 100 ns (20 m), the resulting spectral width is sub mini Hertz. The fractional power contained in  $\Delta f_{FWHM}$  is  $\Delta f_{FWHM} S_{RF}(0) = 64\%$ .

From Eq. (26a) one can also see that for fixed  $\rho_N$  and  $G_A$ , the spectral width of a LIMO is inversely proportional to the oscillation power, similar to the famous Schawlow-Townes formula<sup>23,24</sup> for describing the spectral width  $\Delta \nu_{laser}$  of a laser:

$$\Delta \nu_{laser} = \frac{1}{2\pi} \frac{\rho_s}{\tau_{laser}^2 P_{laser}}, \quad (26b)$$

where  $\rho_s = h\nu$  is the spontaneous emission noise density of the laser,  $P_{laser}$  is the laser oscillation power, and  $\tau_{laser}$  is the decay time of the laser cavity. However, as will be shown in subsection E, both  $P_{osc}$  and  $\rho_N$  are functions of the photocurrent, the statement that the spectral width of a LIMO is inversely proportional to the oscillation power is only valid when thermal noise dominates in the oscillator at low photocurrent levels.

The quality factor  $Q$  of the oscillator from Eq. (26a) is

$$Q = \frac{f_{osc}}{\Delta f_{FWHM}} = Q_D \frac{\tau}{\delta}, \quad (27)$$

where  $Q_D$  is the quality factor of the loop delay line and is defined as:

$$Q_D = 2\pi f_{osc} \tau \quad (28)$$

From Eq. (24b) we easily obtain:

$$S_{RF}(f') = \frac{4\tau^2}{\delta} \quad |f'| \ll \Delta f_{FWHM}/2 \quad (29a)$$

$$S_{RF}(f') = \frac{\delta}{(2\pi)^2 (\tau f')^2} \quad |f'| \gg \Delta f_{FWHM}/2 \quad (29b)$$

It can be shown<sup>25</sup> that for an oscillator with a phase fluctuation much less than unity, its power spectral density is equal to the sum of the single side band phase noise density and the single side band amplitude noise density. In most cases in which the amplitude fluctuation is much less than the phase fluctuation, the power spectral density is just the single side band phase noise. Therefore, it is evident from Eq. (29b) that the phase noise of the LIMO decreases quadratically with the frequency offset  $f'$ . For a fixed  $f'$ , the phase noise decreases quadratically with the loop delay time. The larger the  $\tau$ , the smaller the phase noise. However, the phase noise cannot decrease to zero no matter how large  $\tau$  is, because at large enough  $\tau$ , Eq. (24b) and Eq. (29b) are not valid anymore. From Eq. (24a), the minimum phase noise is  $S_{KF}^{min} \approx \delta/4$  at  $f' = 1/2\tau$ . For the frequency offset  $f'$  outside of the pass band of the 100p filter (where  $F(f') = 0$ ), the phase noise is simply the noise to signal ratio  $\delta$ , as can be seen from Eq. (21).

Eq. (24) and Eq. (29b) also indicate that the oscillator's phase noise is independent of the oscillation frequency  $f_{osc}$ . This result is significant because it allows the generation of high frequency and low phase noise signals with the LIMO. The phase noise of a signal generated using frequency multiplying methods generally increases quadratically with the frequency.

#### E. The Noise to Signal Ratio

As mentioned before, the total noise density input to the oscillator is the sum of the thermal noise  $\rho_{thermal} = 4k_B T(NF)$ , the shot noise  $\rho_{shot} = 2eI_{ph}R$ , and the laser's relative intensity noise (RIN)  $\rho_{RIN} = N_{RIN}I_{ph}^2R$  densities:<sup>26,27</sup>

$$\rho_N = 4k_B T(NF) + 2eI_{ph}R + N_{RIN}I_{ph}^2R, \quad (30)$$

where  $k_B$  is the Boltzman constant,  $T$  is the ambient temperature,  $NF$  is the noise factor of the RF amplifier,  $e$  is the electron charge,  $I_{ph}$  is the photocurrent across the load resistor of the photodetector, and  $N_{RIN}$  is the RIN of the **pump** laser.

From Eq. (25) and Eq. (30) one can see that if the thermal noise is dominant, then  $\delta$  is inversely proportional to the oscillating power  $P_{osc}$  of the oscillator. In general,  $P_{osc}$  is a function of photocurrent  $I_{ph}$  and amplifier gain  $GA$ , as determined by Eq. (17), and the noise to signal ratio from Eq. (25) is thus

$$\delta = \frac{1}{I} \left[ \frac{1}{|G_s|} \frac{4kT(NI^2) + 2eI_p R + \frac{N}{RIN} I_{ph}^2 R}{4\eta^2 \cos^2(\pi V_B/V_\pi) I_{ph}^2 R} \right] \quad (31)$$

In deriving Eq.(31), Eq.(4) and Eq.(17b) are used. From Eq.(31) one can see that  $\delta$  is a nonlinear function of the small signal gain of the oscillator. As shown in Fig. 5a, it reaches the minimum value at  $|G_s| = 3/2$ :

$$\delta_{\min} = \frac{4kT(NI^2) + 2eI_p R + \frac{N}{RIN} I_{ph}^2 R}{(16/27) I_{ph}^2 R}, \quad (32)$$

where  $\eta = 1$  and  $\cos(\pi V_B/V_\pi) = 1$  are assumed. The oscillation amplitude at  $|G_s| = 3/2$  can be obtained from Eq. (17b) to be

$$V_{osc} = 2\sqrt{2}V_\pi/(\pi\sqrt{3}) \approx 0.52V_\pi, \quad (33a)$$

and the corresponding RF power is

$$P_{osc} = 4V_\pi^2/(3\pi^2 R) = 10P_m^{1dB}/3, \quad (33b)$$

where  $P_m^{1dB}$  is the input 1 dB compression power of the E/O modulator.<sup>27,28</sup> From Eq (33b) one can conclude that in order to have minimum noise, the oscillation power measured at the input of the E/O modulator should be 5 dB above the 1 dB compression power of the modulator. Eq.(33a) indicates that the noise of the oscillator is minimum when the oscillating amplitude is roughly half  $V_\pi$  or the voltage in the oscillator is varying between the peak and the trough of the sinusoidal transmission curve of the E/O modulator. This makes sense because the modulator has its minimum sensitivity to voltage variations at the maximum and the minimum of the transmission curve, and the most likely cause of voltage variations in a LIMO is the noise in the loop.

It is evident from Eq.(32) that the higher the photocurrent, the less the noise to signal ratio of the oscillator until it flattens out at the laser's RIN level. Therefore, the ultimate noise to signal ratio of a LIMO is limited by the pump laser's RIN. If the RIN of the pump laser in a LIMO is -160 dB/Hz, the ultimate noise to signal ratio of the oscillator is also -160 dB/Hz and the signal to noise ratio is 160 dB/Hz. Fig.5b shows the noise to signal ratio  $\delta$  as a function of photocurrent  $I_{ph}$  for different RIN levels. in the plot, the small signal gain  $G_s$  is chosen to be a constant of 1.5, which implies that when  $I_{ph}$  is increased, the amplifier gain  $G_A$  must be



decreased to keep  $G_s$  constant. From the figure one can easily see that  $\delta$  decreases quadratically with  $I_{ph}$  at small  $I_{ph}$  and flattens out at the RIN level at large  $I_{ph}$ .

### F. Effects of Amplifier's Nonlinearity

In the discussions above, we have assumed that the nonlinear distortion of a signal from the E/O modulator is more severe than from the amplifier (if any) used in the oscillator so that the oscillation amplitude or power is limited by the nonlinear response of the E/O modulator. Using an engineering term, this simply means that the output 1 dB compression power of the amplifier is much larger than the input 1 dB compression power of the E/O modulator.<sup>27</sup>

For cases **in which** the output 1 dB compression power of the amplifier is less than the input 1 dB compression power of the modulator, the nonlinearity of the amplifier will limit the oscillation amplitude  $V_{osc}$  (or power  $P_{osc}$ ) of the oscillator, resulting in an oscillation amplitude less than that given by Eq. (17). The exact relation between the oscillation amplitude (or power) and the small signal gain  $G_s$  can be determined using the same linearization procedure as that for obtaining Eq. (17) if the nonlinear response function of the amplifier is known. However, all the equations in subsection D for describing the spectrum of the oscillator are still valid, provided that the oscillation power in those equations is determined by the nonlinearity of the amplifier. For a high enough small signal gain  $G_s$ , the oscillation power is approximately a few dB above the output 1 dB compression power of the amplifier.

In all the experiments discussed below, the output 1 dB compression power of the amplifiers chosen is much larger than the input 1 dB compression power of the modulator so that the oscillation power is limited by the modulator.

## EXPERIMENTS

### A. Amplitude vs. Open Loop Gain

We performed measurements to test the level of agreement of the theory described above with experimental results. In all of our experiments, we used a highly stable diode-pumped Nd:YAG ring laser<sup>24</sup> with a built-in RIN reduction circuit<sup>29</sup> to pump the LIMO. The experimental setup for measuring the oscillation amplitude as a function of the open loop gain is shown in Fig. 6a. Here an RF switch was used to

open and close the loop. While the loop was open, an RF signal from a signal generator with the same frequency as the oscillator was injected into the E/O modulator. The amplitudes of the injected signal and the output signal from the loop was measured with an oscilloscope to obtain the open loop gain which was the ratio of the output amplitude to the injected signal amplitude. The open loop gain was varied by changing the bias voltage of the E/O modulator, or by attenuating the optical power of the loop, or by using a variable RF attenuator after the photodetector, as indicated by Eq. (4). When closing the loop, the amplitude of the oscillation was conveniently measured using the same oscilloscope. We measured the oscillation amplitudes of the LIMO for different open loop gains at an oscillation frequency of 100 MHz, and the data obtained is plotted in Fig. 4b. It is evident that the experimental data agrees well with our theoretical predictions.

### B. The Phase Noise Measurement Setup

We used the frequency discriminator method<sup>30</sup> to measure the phase noise of the LIMO and the experimental setup is shown in Fig. 6b. The advantage of this method is that it does not require a frequency reference and hence can be used to measure an oscillator of any frequency. Using a microwave mixer in the experiment we compared the phase of a signal from the electrical output port of the LIMO with its delayed replica from the optical output port. The length of the delay line is important because the longer the delay line the lower the frequency offset at which the phase noise can be accurately measured. On the other hand, if the delay line is too long, the accuracy of the phase noise at higher frequency offset will suffer. The length of delay used in our experiment is 1 km or 5  $\mu$ s. Because of this delay, any frequency fluctuation of the LIMO will cause a voltage fluctuation at the output of the mixer. We measured the spectrum of this voltage fluctuation with a high dynamic range spectrum analyzer and transferred the spectral data to a computer. Finally, we converted this information into the phase noise spectrum of the LIMO according to the procedures given in reference 30. In these experiments, the noise figure of the RF amplifier was 7 dB.

### C. Phase Noise as a Function of Offset Frequency and Loop Delay

Fig. 7a is the log vs log scale plot of the measured phase noise as a function of the frequency offset  $f'$ . Each curve corresponds to a different loop delay time. Clearly,

the phase noise has a 20dB per decade dependence on the frequency offset, in excellent agreement with the theoretical prediction of Eq. (29 b).

Fig. 7b is the **measured phase noise at 30 kHz from the center frequency as a function** of the loop delay time, extracted from the different curves of Fig. 7a. Because the loop delay is increased by adding more fiber segments, the open loop gains of the oscillator with longer loops decrease as more segments are connected, causing the corresponding oscillation power to decrease. From the results of Fig. 9 below, the phase noise of the LIMO decreases linearly with the oscillation power. To extrapolate the dependence of the phase noise on the loop delay only from Fig. 7a, each data point in Fig. 7b is calibrated using the linear dependence of Fig. 9, while keeping the oscillation power for all data points at  $-16.33\text{ mW}$ . Again, the experimental data agrees well with the theoretical prediction.

#### D. Phase Noise Independence of Oscillation Frequency

To confirm our prediction that the phase noise of the LIMO is independent of the oscillation frequency, we measured the phase noise spectrum as a function of the oscillation frequency and the result is shown in Fig. 8a. In the experiment, we kept the loop length at  $0.28\text{ }\mu\text{s}$  and varied the oscillation frequency by changing the RF filter in the loop. The frequency was fine tuned using an RF line stretcher. It is evident from Fig. 8a that all phase noise curves at frequencies 100 MHz, 300 MHz, 700 MHz, and 800 MHz overlap with one another, indicating a good agreement with the theory. Fig. 8b is a plot of the phase noise data at 10 kHz as a function of the frequency. As predicted, it is a flat line, in contrast with the case when a frequency multiplier is used to obtain higher frequencies. This result is significant because it confirms that the LIMO can be used to generate high frequency signals up to 75 GHz with a much lower phase noise than that can be attained with frequency multiplying techniques.

#### E. Phase Noise as a Function of Oscillation Power

We have also measured the phase noise spectrum of the LIMO as a function of oscillation power with the results shown in Fig. 9. In this experiment, the loop delay of the LIMO was  $0.06\text{ }\mu\text{s}$ , the noise figure of the RF amplifier was 7 dB, and the oscillation power was varied by changing the photocurrent  $I_{ph}$  according to Eqs. (3), (4), and (17). With this amplifier and the photocurrent level (1.8 mA -2.7 mA), the

thermal noise in the oscillator dominates. Recall that in Eq. (24) and Eq. (25), the phase noise of a LIMO is shown to be inversely proportional to the oscillation power. This is true if the gain of the amplifier is kept constant and the photocurrent is low enough to ensure that the thermal noise is the dominant noise term. In Fig. 9a, each curve is the measurement data of the phase noise spectrum corresponding to an oscillating power and the curves in Fig. 9b are the fits of the data to Eq.(29b). Fig. 9c is the phase noise of the LIMO at 10kHz as a function of the oscillation power, extracted from the data of Fig. 9b. The resulting linear dependence agrees well with the theoretical prediction of Eq.(29b).

## SUMMARY

We have introduced a high frequency, high stability, high spectral purity, widely tunable electro-optic oscillator which we have termed LIMO. The high stability and spectral purity of the LIMO result from the extremely low energy storage loss realization obtained with a long optical fiber. The optical fiber is also virtually free of any frequency dependent loss, resulting in the same long storage time and high spectral purity signals for both low and high frequency oscillations. On the other hand, the oscillation frequency of the LIMO is only limited by the speed of the modulator, which at the present can be as high as 75GHz. As yet another unique feature, the output of the LIMO may be obtained directly as microwave signals, or as intensity modulations on an optical carrier for easy interface with optical systems.

We also analyzed the performance of this oscillator by deriving expressions for the oscillation threshold Eq. (5), oscillation amplitude Eq. (17), and oscillation frequency Eq. (18). This result agrees quite well with experimental data obtained with laboratory versions of the LIMO.

We derived the expression for the spectrum of the output of the LIMO and showed that it has a Lorentzian line shape, given by Eq.(24). The spectral width of the output signal was found to be inversely proportional to the square of the loop delay time, given by Eq. (26). In addition, at low optical pumping levels where thermal noise dominates, the spectral linewidth was found to be inversely proportional to the oscillation power of the oscillator, similar to the Schawlow-Townes formula describing the spectral width of a laser. Since increasing the optical pump power increases the oscillation power, in this regime the linewidth of the LIMO decreases as the optical pump power increases. On the other hand, at high pump powers

where the pump laser's relative intensity noise dominates, the spectral width approaches a minimum value determined by the laser's RIN noise, as given by Eq. (24) and Eq. (32). We measured the phase noise spectrum of the LIMO and verified our theoretical findings.

It is important to note that the analysis performed here was for the specific case of the LIMO with a Mach Zehnder electro-optic modulator. Other modulation schemes such as with electro-absorptive modulators or the direct modulation of semiconductor lasers<sup>31</sup> will also lead to signals with characteristics similar to those obtained in this work. For these cases the theoretical approach developed above is still applicable after suitable modifications. The major change required in the analysis is the replacement of Eq. (1) which describes the transmission characteristics of a Mach Zehnder modulator with the appropriate equation for the specific modulation scheme. All other equations can then be derived in the same way as described in the theory.

Because of its unique properties, the LIMO may be used in a number of applications. As a voltage controlled oscillator,<sup>12</sup> it can perform all the VCO functions in both electronic and photonic applications including generating, tracking, and cleaning RF carriers. The LIMO has the unique property of actually amplifying injected signals,<sup>12</sup> and thus may be used in high frequency carrier regeneration and signal amplification. Other important potential applications of the LIMO include high speed clock recovery,<sup>32,33</sup> comb and pulse generation,<sup>12</sup> high gain frequency multiplication, and photonic signal up and down conversion<sup>34</sup> in photonic RF systems.<sup>35,36</sup>

#### ACKNOWLEDGEMENT

We thank G. Lutes and C. Greenhall for many helpful discussions, and M. Calhoun for lending us many key components in experiments.

## REFERENCES

1. J. Marion and W. Hornyak, *Physics for Science and Engineering* (Saunders College Publishing, Philadelphia, 1982), Ch. 15.
2. B. van der Pol, "A theory of the amplitude of free and forced triode vibrations," *Radio Review*, Vol. 7, pp. 701-754 (1920).
3. van der Pol, "The nonlinear theory of electric oscillations," *Proceedings of the Institute of Radio Engineers*, Vol. 22, No. 9, pp. 1051-1086 (1934).
- 4.0. Ishihara et al., "A highly stabilized GaAs FET oscillator using a dielectric resonator feedback circuit in 9-14 GHz," *IEEE Trans. Microwave Theory Tech.* Vol. MTT-28, No. 8, pp. 817-824 (1980).
5. Siegman, *Microwave Solid State Masers* (McGraw-Hill, 1964).
6. Siegman, *Lasers* (University Science Books, Mill Valley, 1986), Ch. 11.
7. A. Ballato, "Piezoelectric resonators," in *Design of Crystal and Other Harmonic Oscillators*, B. Parzen, ed. (John Wiley and Sons, 1983), pp. 66-122.
8. W. L. Smith, "Precision oscillators," in *Precision Frequency Control*, Vol. 2, E. A. Gerber and A. Ballato, ed. (Academic Press, 1985), pp. 45-98.
9. J. K. Plourde and C. R. Ren, "Application of dielectric resonators," *IEEE Trans. Microwave Theory Tech.*, Vol. MTT-29, No. 8, pp. 754-769 (1981).
10. M. W. Lawrence, "Surface acoustic wave oscillators," *Wave Electronics*, Vol. 2, pp. 199-218 (1976).
11. X. Steve Yao and Lute Maleki, "High frequency optical subcarrier generator," *Electron. Lett.* 30 (18), pp. 1525-1526 (1994).
12. X. Steve Yao and Lute Maleki, "A novel photonic oscillator," *The Telecommunication and Data Acquisition Progress Report 42-121*, Vol. April-June, Jet Propulsion Laboratory, Pasadena, California, pp. 32-42 (1995), obtainable at [http://tda.jpl.nasa.gov/progress\\_report](http://tda.jpl.nasa.gov/progress_report). Also in *the LEOS Summer Topical Meetings, 1995 Digest of the LEOS Summer Topical Meetings* (Institute of Electrical

and Electronics Engineering, Piscataway, NJ. IEEE catalog number 95TH 18031 ), RF optoelectronics pp. 17-18.

13. M. Rodwell, J. E. Bowers, R. Pallela, K. Gilboney, J. Pust, and D. Nguyen, "Electronic and optoelectronic components for fiber transmission at bandwidths approaching 100 GHz," in *the IEEE Summer Topical Meetings, 1995 Digest of the IEEE Summer Topical Meetings* (Institute of Electrical and Electronics Engineering, Piscataway, NJ. IEEE catalog number 95TH 18031), RF Optoelectronics pp. 21-22.

14. K. Noguchi, H. Miyazawa, and O. Mitomi, "75 GHz broadband Ti:LiNbO<sub>3</sub> optical modulator with ridge structure," *Electron. Lett.* Vol. 30, No. 12, pp. 949-951 (1994).

15. A. Neyer and E. Voges, "Nonlinear electrooptic oscillator using an integrated interferometer," *Opt. Commun.*, 37, pp. 169-174 (1980)

16. A. Neyer and E. Voges, "Dynamics of electrooptic bistable devices with delayed feedback," *IEEE J. Quantum Electron.*, QE-18(12), pp. 2009-2015 (1982).

17.11. F. Schlaak and R. Th. Kersten, "Integrated optical oscillators and their applications to optical communication systems," *Optics Communications*, Vol. 36, No. 3, pp. 186-188, (1981).

18.11. M. Gibbs, F. A. Hopf, D. L. Kaplan, M. W. Derstine, R. L. Shoemaker, "Periodic oscillation and chaos in optical bistability: possible guided wave all optical square-wave oscillators," *SPIE Proceedings Vol. 317, Integrated Optics and Millimeter and Microwave integrated Circuits*, pp. 297-304.

19. E. Garmire, J. H. Marburger, S. D. Allen, and H. G. Winful, "Transient response of hybrid bistable optical devices," *Appl. Phys. Lett.*, Vol. 34, No. 6, pp. 374-376, (1979).

20. Neyer and E. Voges, "High-frequency electro-optic oscillator using an integrated interferometer," *Appl. Phys. Lett.*, vol. 40, No. 1, pp. 6-8, (1982).

21. T. Aida and P. Davis, "Applicability of bifurcation to chaos: Experimental demonstration of methods for switching among multistable modes in a nonlinear resonator," in *OSA proceedings on Nonlinear Dynamics in optical Systems*, ed. N. B. Abraham, E. Garmire, and P. Mandel, Vol. 7, pp. 540-544, Optical Society of America (1990)

22. M. F. Lewis, "Some aspects of saw oscillators," Proc. of 1973 Ultrasonics symposium, IEEE, 1973, pp 344-347.
23. A. L. Schawlow and C. H. Townes, "Infrared and optical masers," Phys. Rev. Vol. 112, No. 6, pp. 1940-1949 (1958).
24. R. L. Byer, "Diode laser-pumped solid-state lasers," Science, Vol. 239, pp. 742-747 (1988).
25. S. C. Culter and C. L. Searle, "Some aspects of the theory and measurement of frequency fluctuations in frequency standards," 1 'proceedings of the IEEE, vol. 54, No. 2, pp 136-154, 1966.
26. A. Yariv, *introduction to Optical Electronics, second edition* (Holt, Rinehart and Winston, New York, 1976), Ch. 10.
27. X. S. Yao and L. Maleki, 'Influence of an externally modulated photonic link on a microwave communications system,' The Telecommunication and Data Acquisition Progress Report 42-117, Vol. January-March, Jet Propulsion Laboratory, Pasadena, California, pp 16-28 (May 15, 1994), obtainable at [http://tda.jpl.nasa.gov/progress\\_report](http://tda.jpl.nasa.gov/progress_report),
28. X. S. Yao and L. Maleki, 'Field demonstration of X-band photonic antenna remoting in the deep space network,' The Telecommunication and Data Acquisition Progress Report 42-117, Vol. January-March 1994, Jet Propulsion Laboratory, Pasadena, California, pp. 29-34 (May 15, 1994), obtainable at [http://tda.jpl.nasa.gov/progress\\_report](http://tda.jpl.nasa.gov/progress_report).
29. T. J. Kane, "Intensity noise in diode-pumped single-frequency Nd:YAG lasers and its control by electronic feedback," IEEE Photon. Technol. Lett., Vol. 2, No. 4, pp. 244-245 (1990).
30. Hewlett-Packard Co., "Phase noise characterization of microwave oscillators - Frequency discriminator method," Product note 11729C-2.
31. M. F. Lewis, "Novel RF oscillator using optical components," Electron. Lett. Vol. 28, No. 1, pp. 31-32 (1992).
32. X. Steve Yao and George Lutes, 'A high speed photonic clock and carrier regenerator,' The Telecommunication and Data Acquisition Progress Report, 42-121,



Vol. January-March 1994, Jet Propulsion Laboratory, Pasadena, California, pp. 202-209 (May 15, 1995), obtainable at [http://tda.jpl.nasa.gov/progress\\_report](http://tda.jpl.nasa.gov/progress_report).

33. X. Steve Yao, George Lutes, Lute Maleki, and Simon Cao, "A novel photonic clock and carrier recovery device," SPIE Proceedings Vol. 2556, Wireless Communications, pp. 118-127 (1995).

34. G. K. Gopalakrishnan, W. K. Hums, and C. H. Bulmer, 'Microwave-optical mixing in LiNbO<sub>3</sub> modulators," IEEE Trans. Microwave Theory Techn., 41(12), pp. 2383-2391 (1993).

35. I. Ogawa, D. Polifko, and S. Banba, 'Millimeter-wave fiber optics systems for personal radio communication,' IEEE Trans. Microwave Theory Techn., 40(12), pp. 2285-2293 (1992).

36. P. Herczfeld and A. Daryoush, "Fiber optic feed network for large aperture phased array antennas," Microwave Journal, August 1987, pp. 160-166.

## FIGURE CAPTIONS

Fig. 1 Comparison of a van der Pol oscillator (a) with a light induced microwave oscillator (b).

Fig. 2 Detailed construction of a LIMO. optical injection and RF injection ports are supplied for synchronizing the oscillator with an external reference by either optical injection locking or electrical injection locking.<sup>12</sup> The bias port and the fiber stretcher can be used to fine tune the oscillation frequency. Noise in the oscillator can be viewed as being injected from the input of the amplifier.

Fig. 3 Illustration of the oscillator's output spectra below and above the threshold.

Fig. 4 Normalized oscillation amplitude of a LIMO as a function of small signal gain  $G_s$ . (a) Theoretical calculation using Eqs. (17a), (17b), and (17c). (b) Experimental data and curve fitting to Eq.(17b) and Eq. (17c).

Fig. 5 Calculations of LIMO's input noise to signal ratio. (a) input noise to signal ratio as a function of small signal gain  $G_s$ , showing a minimum value at  $G_s = 1.5$ . (b) input noise to signal ratio as a function of photocurrent for different values of laser's RIN noise. in the calculation, the noise factor of the RF amplifier is assumed to be 2 and  $G_s$  is fixed at 1.5.

Fig. 6 Experimental setups. (a) For measuring the oscillation amplitude of a LIMO as a function of the small signal gain. (b) For measuring the phase noise of a LIMO using frequency discrimination method.

Fig. 7 Single side band phase noise of a LIMO measured at 800 MHz. (a) Measured phase noise spectra at different loop delays and their fits to Eq.(29b). The corresponding loop delays for curves 1 -5 are listed adjacent to each curve and the corresponding oscillation powers are 16.33, 16, 15.67, 15.67, and 13.33 dBm respectively. Curve fitting yields the following phase noise relations as a function of frequency offset  $f'$ :  $-28.7 - 20 \log(f')$ ,  $-34.84 - 20 \log(f')$ ,  $-38.14 - 20 \log(f')$ ,  $-40.61 - 20 \log(f')$ , and  $-50.45 - 20 \log(f')$ . (b) Phase noise at 30 kHz offset from the center frequency as a function of loop delay. Data points were extracted from curves 1-5 of (a) and were corrected to account for oscillation power differences.

Fig. 8 Single side band phase noise measurements of the LIMO at different oscillation frequencies. (a) Phase noise spectra. (b) 1<sup>st</sup> base noise at 10 kHz offset frequency as a function of oscillation frequency, extracted from (a). The loop delay for the measurements is 0.28 ps.

Fig. 9 Single side band phase noise spectra as a function of oscillation power measured at 800 MHz. (a) Experimental data. (b) The fit to Eq.(29b). (c) Phase noise at 10 kHz offset as a function of oscillation power extracted from (b).

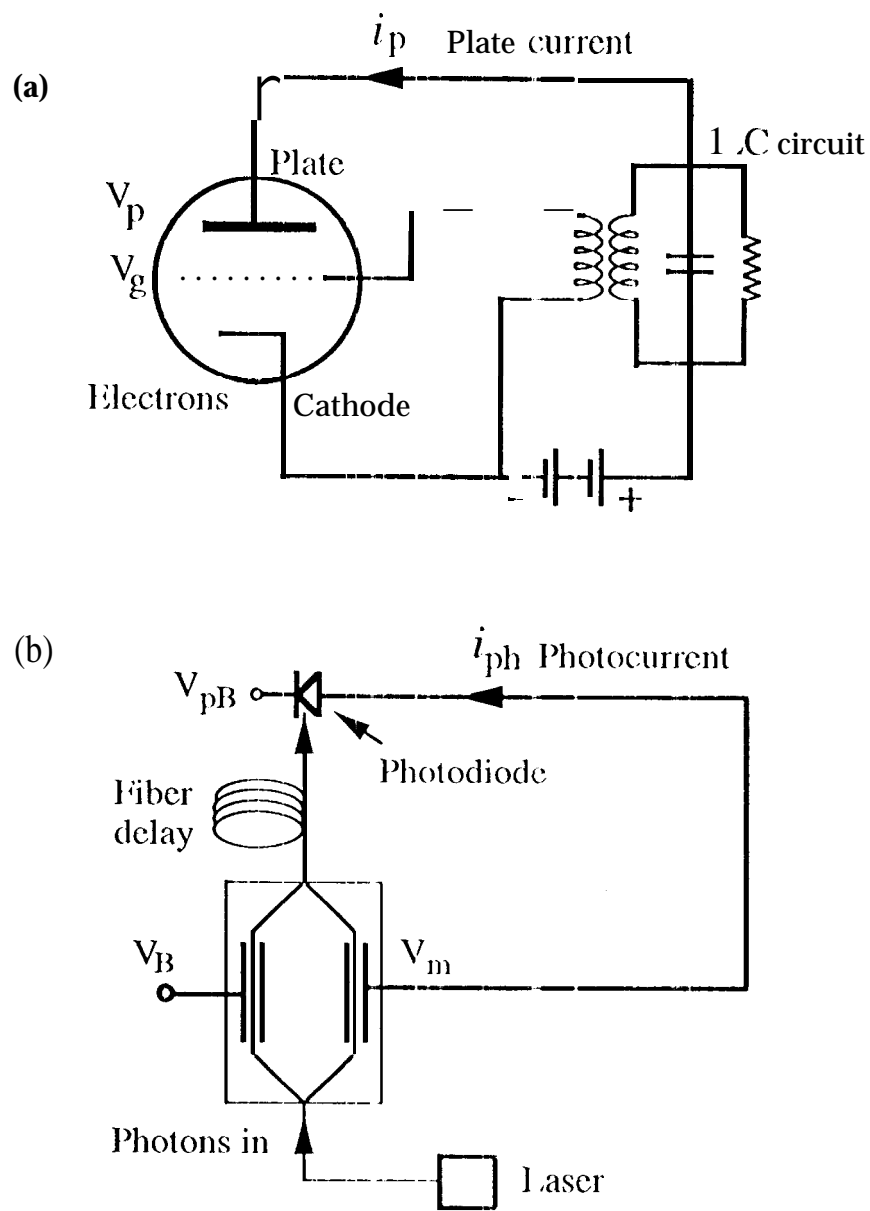


Fig. 1

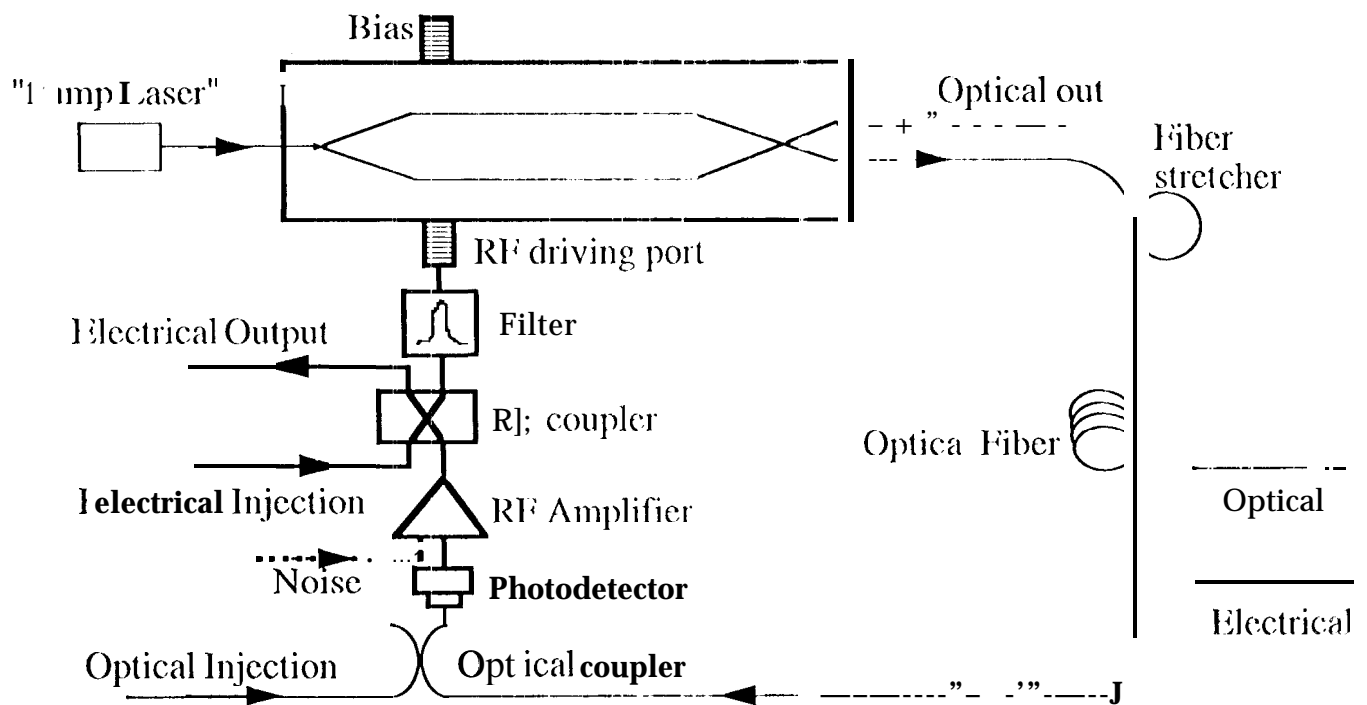


Fig. 2

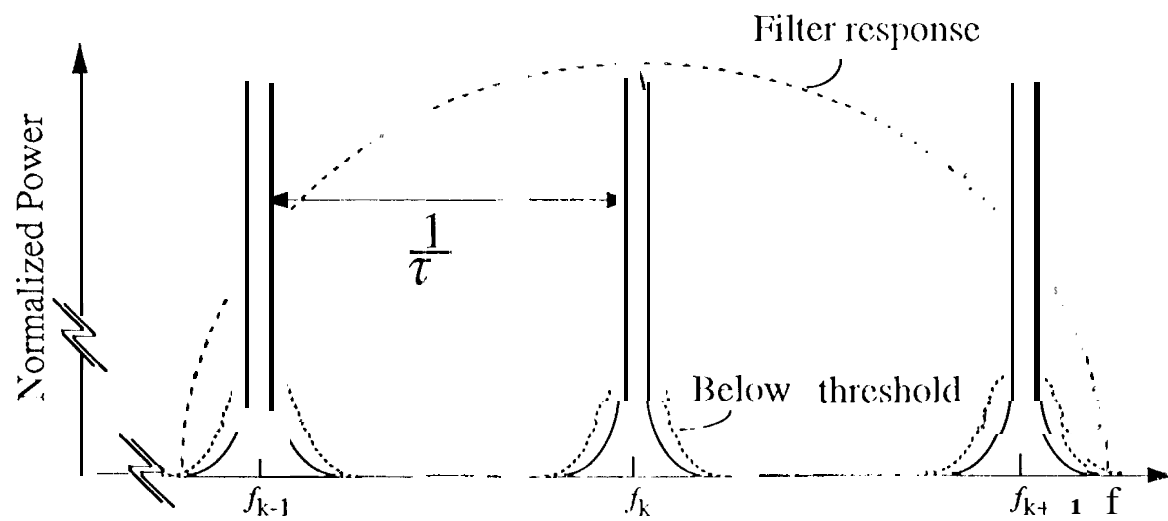


Fig. 3

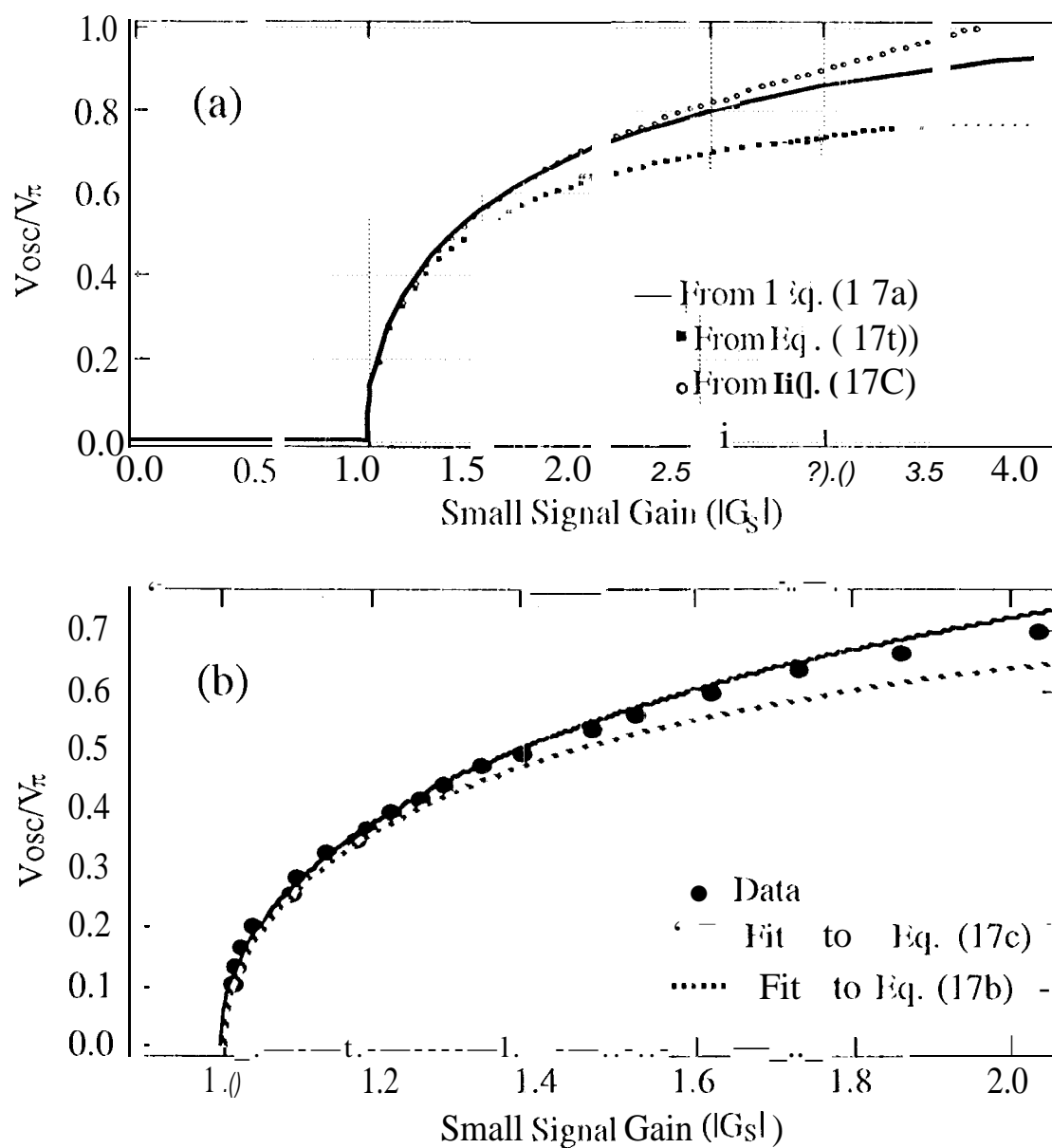


Fig. 4

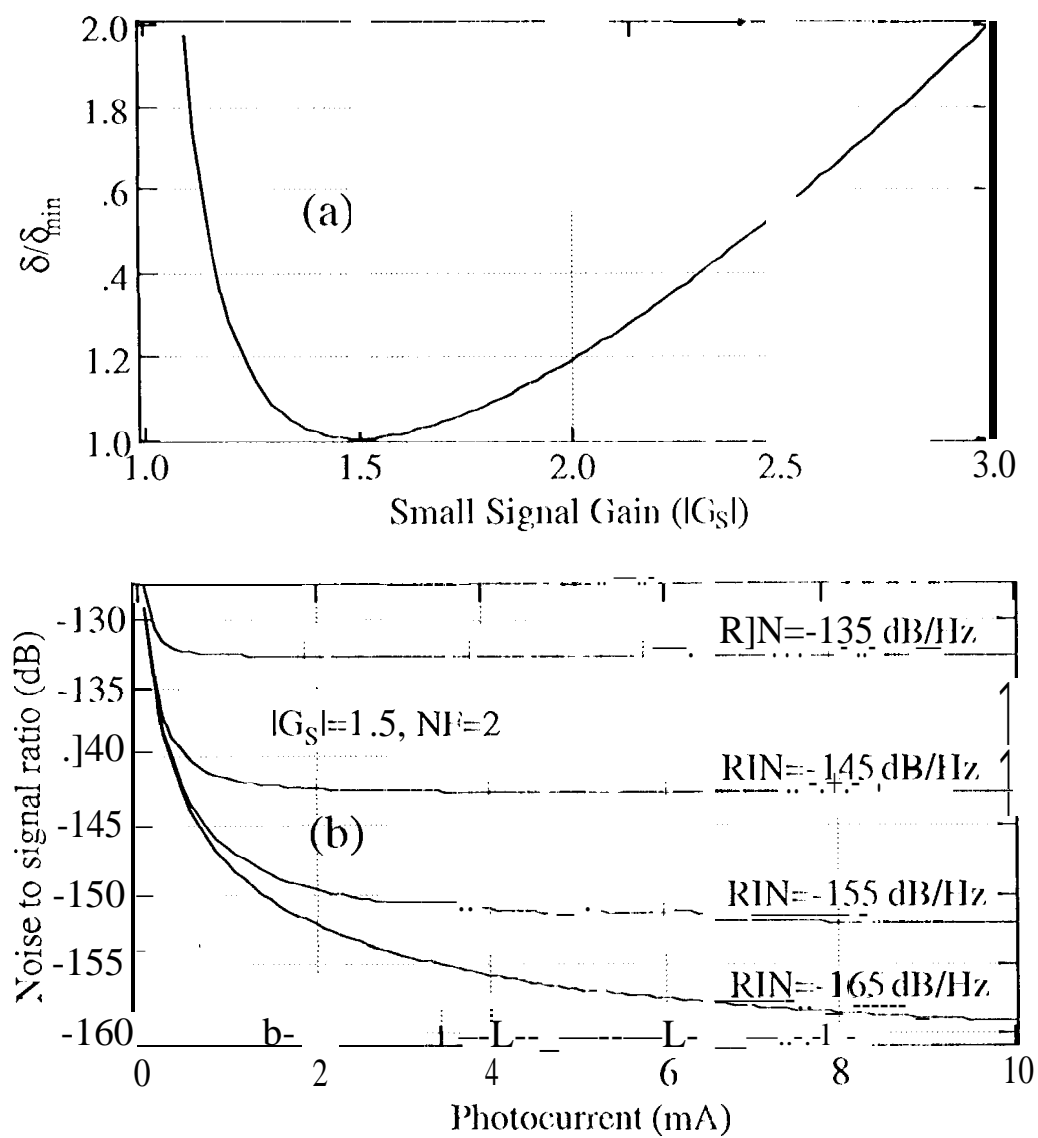


Fig. 5



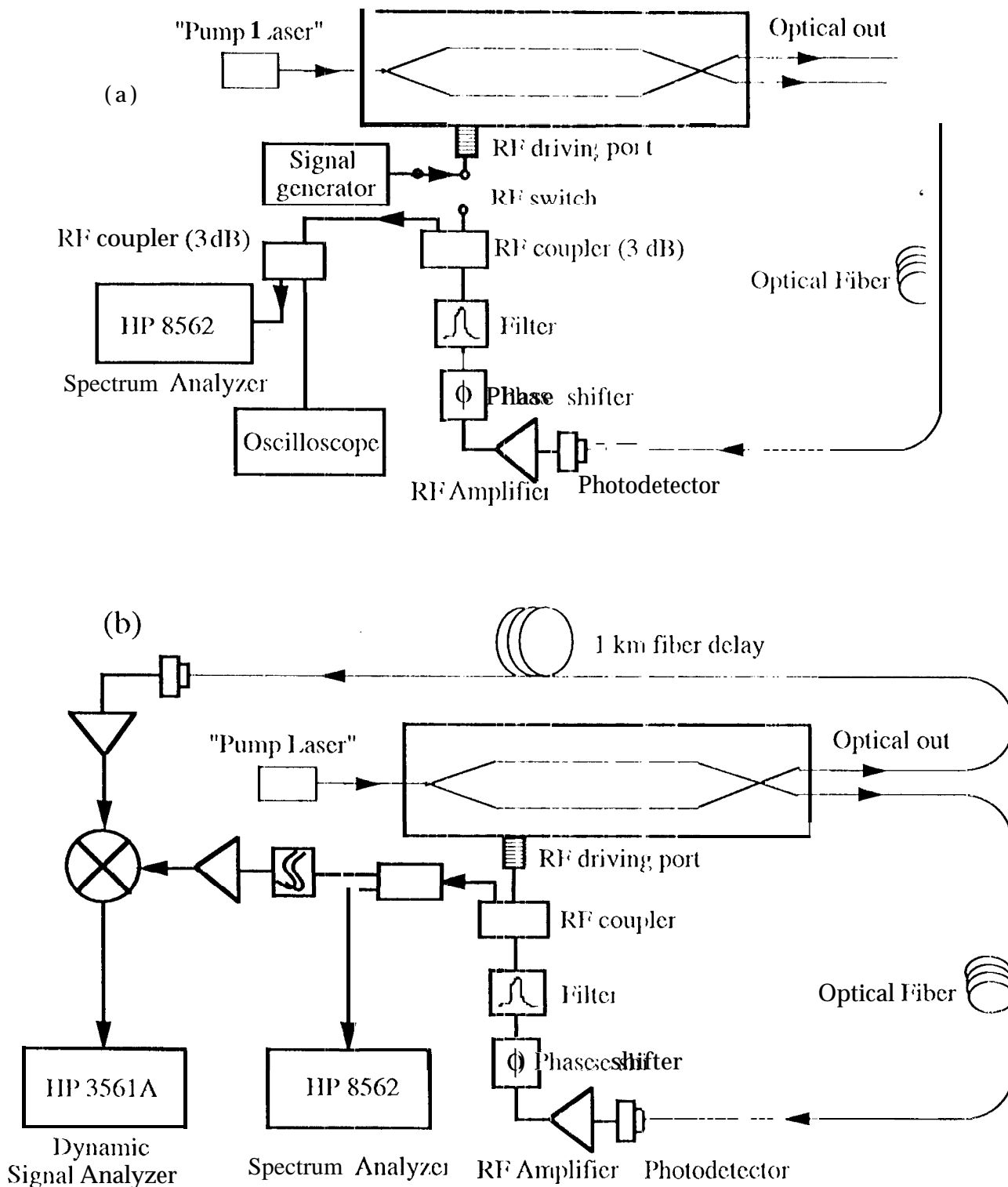


Fig. 6

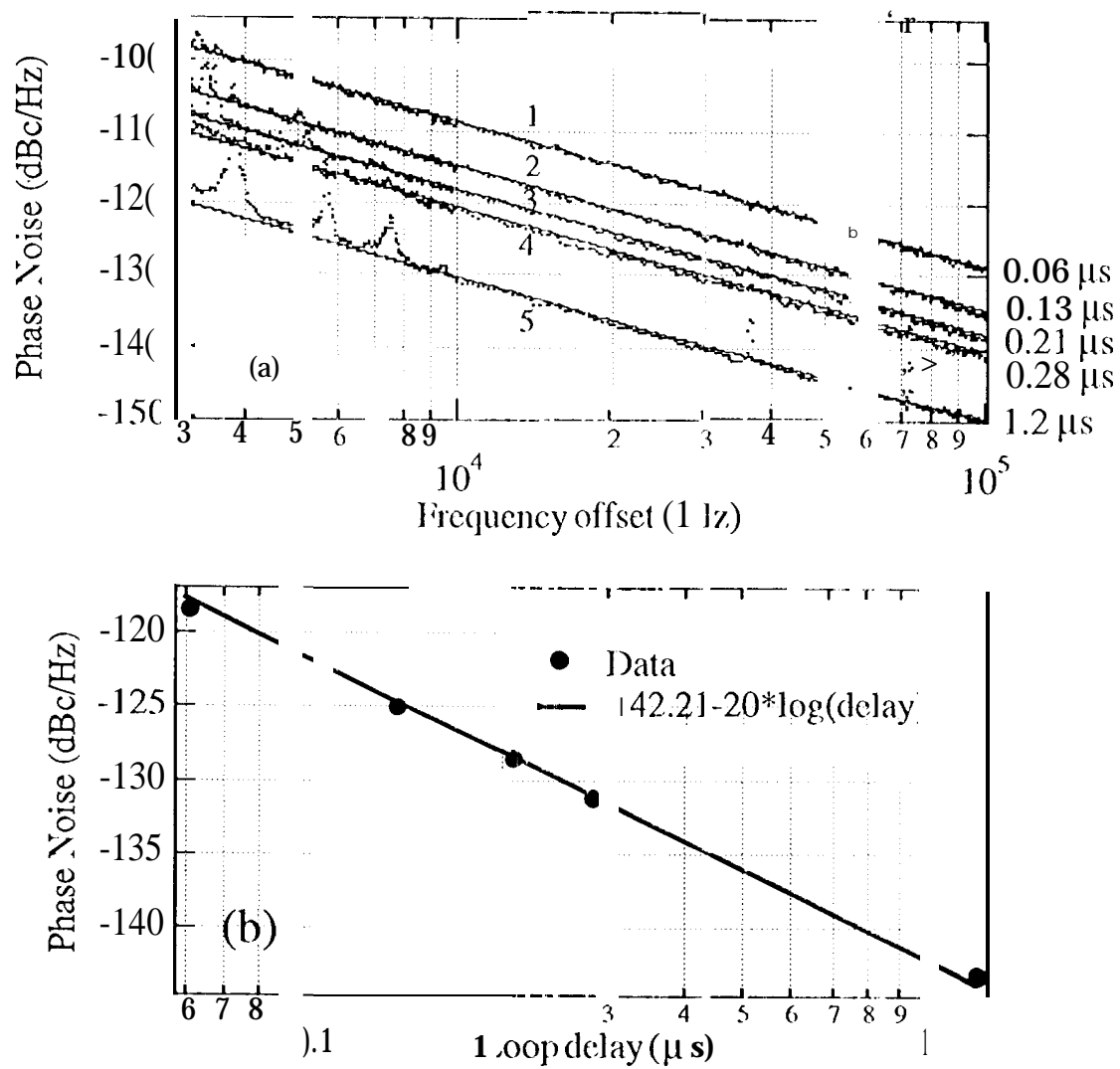


Fig. 7

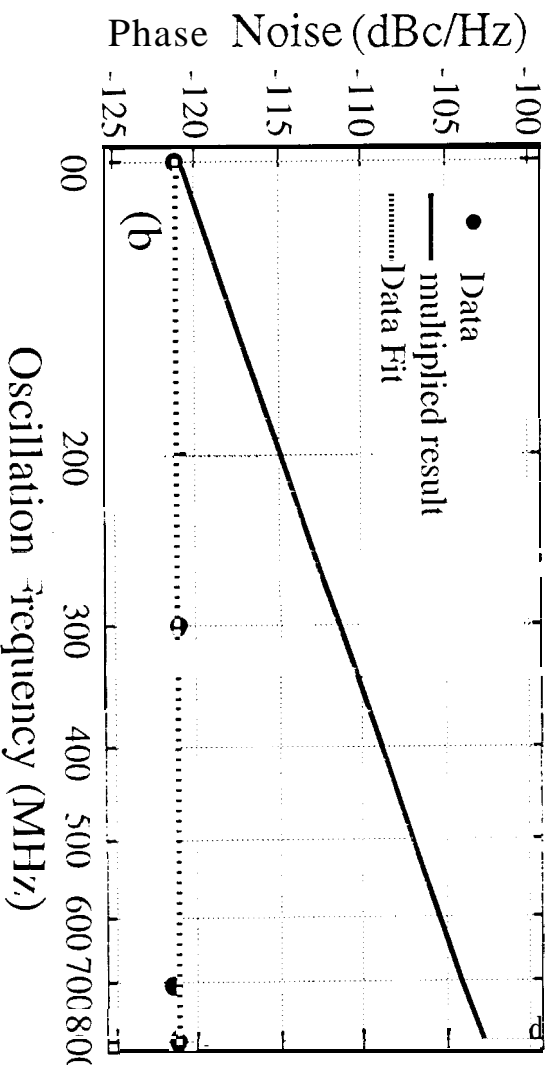
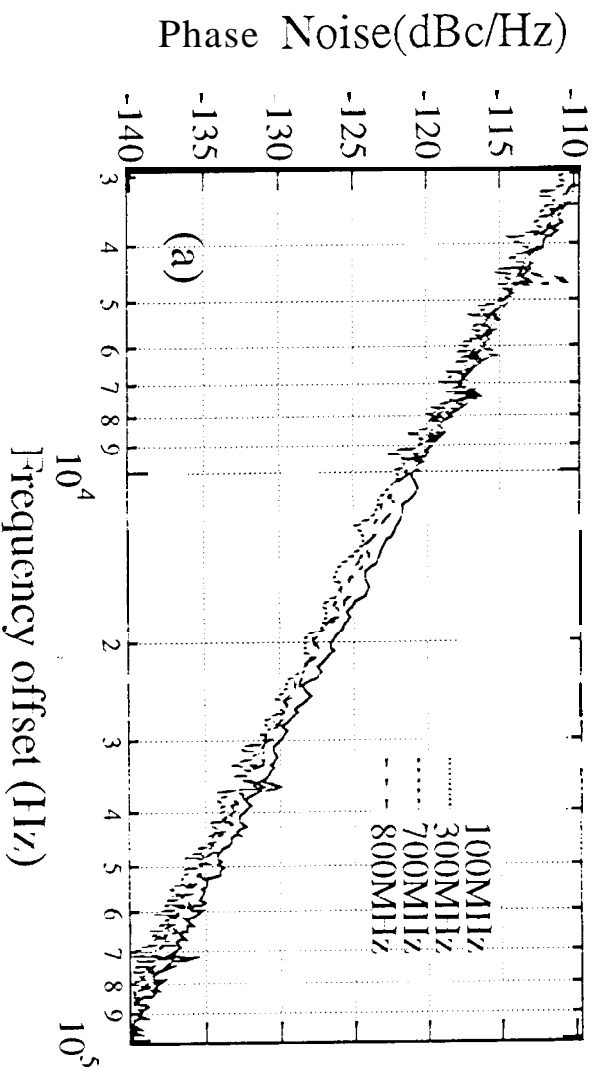


Fig. 8

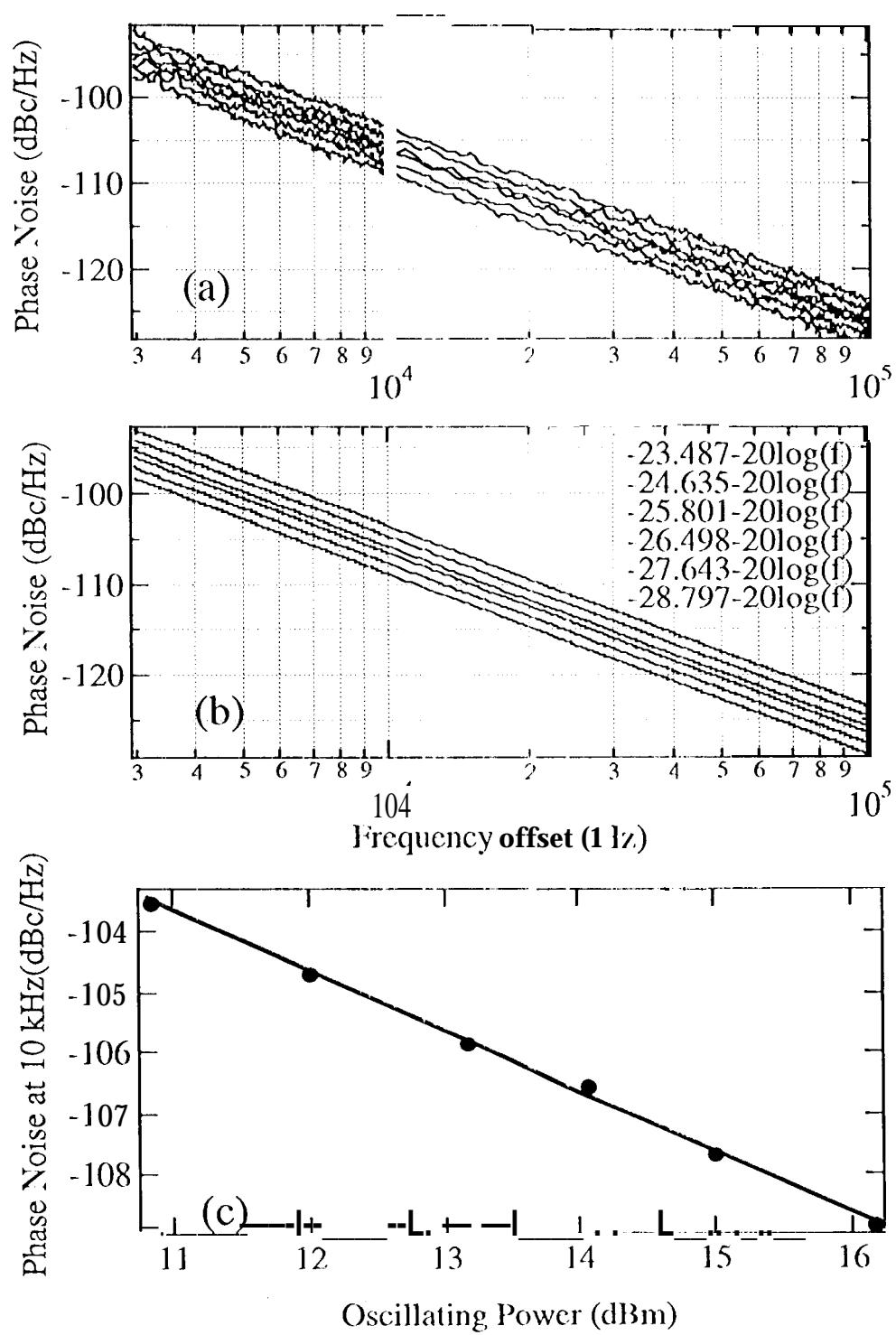


Fig. 9